ELSEVIER

Biomaterials 23 (2002) 4863–4871

Biomaterials

www.elsevier.com/locate/biomaterials

Surface oxidation of NiTi shape memory alloy

G.S. Firstov*, R.G. Vitchev[1], H. Kumar, B. Blanpain, J. Van Humbeeck

Katholieke Universiteit Leuven, MTM, Kasteelpark Arenberg 44, B-3001 Leuven, Belgium

Received 7 May 2002; accepted 10 June 2002

Abstract

Mechanically polished NiTi alloy (50 at% Ni) was subjected to heat treatment in air in the temperature range 300–800°C and characterised by scanning electron microscopy, X-ray diffraction, X-ray photoelectron spectroscopy and Raman spectroscopy. Thermogravimetry measurements were carried out to investigate the kinetics of oxidation. The results of thermodynamic calculations were compared to the experimental observations. It was found that NiTi alloy exhibits different oxidation behaviour at temperatures below and above 500°C. A Ni-free zone was found in the oxide layer for oxidation temperatures of 500°C and 600°C. The oxidation at 500°C produces a smooth protective nickel-free oxide layer with a relatively small amount of Ni species at the air/oxide interface, which is in favour of good biocompatibility of NiTi implants. The oxidation mechanism for the NiTi shape memory alloy is discussed.

Keywords: Oxidation; Intermetallic; Shape memory alloys; Biomaterials

1. Introduction

NiTi shape memory alloys have attracted considerable attention as materials for medical implants [1]. It is known that the biocompatibility of the implants fabricated from NiTi depends on a corrosion resistant titanium oxide layer avoiding the allergic and toxic effects of nickel [2]. However, nickel either in metallic or in oxidised state is also detected on the surface of NiTi, its amount depending on the surface treatment. Several authors [3–7] studied the effect of heat treatment on surface composition of NiTi. In a previous paper [8], the oxide layers formed on NiTi after oxidation in air were studied by X-ray photoelectron spectroscopy (XPS). The purpose of the present study was to determine the conditions of the oxidation for NiTi medical implants that will ensure the surface formation of a protective layer of Ti oxides with the minimal release of Ni through it. In order to achieve such a purpose, a systematic study employing scanning electron microscopy (SEM), X-ray diffraction (XRD), thermogravimetry, XPS and Raman spectroscopy was carried out.

2. Experimental

The Ni-50 at% Ti alloy used in this investigation was induction melted from Ti iodide and electrolytic Ni under argon atmosphere. The kinetics of oxidation was investigated by thermogravimetry (DuPont 951 TGA). Flat specimens (for thermogravimetry measurements), $1.5 \times 1.5 \times 5\,mm^3$ in dimension, were cut from the ingot, mechanically polished with emery paper to a mirror finish and ultrasonically cleaned in demineralised water and ethanol. Thermogravimetric measurements versus temperature were performed with a heating rate of 1°C/min under 50 ml/min air flow. Isothermal thermogravimetry was carried out at 300°C and 800°C for about 10^5 s. The specimens were kept under a 50 ml/min argon flow which was switched to 50 ml/min of air flow at the actual temperature of the isothermal oxidation experiment (300°C or 800°C) in order to prevent oxidation during preliminary heating. Samples of $1 \times 5 \times 20\,mm^3$ were mechanically polished, ultrasonically cleaned in demineralised water and ethanol, oxidised in a furnace in air at several temperatures in the range 300–800°C for half an hour and studied by means of SEM, XRD, XPS

*Corresponding author. Fax: +32-16-32-19-92.
E-mail address: georgiy.firstov@mtm.kuleuven.ac.be (G.S. Firstov).
[1] Present address: Laboratoire Interdisciplinaire de Spectroscopie Electronique (LISE), Facultes Universitaires Notre-Dame de la Paix, Rue de Bruxelles 61, B-5000 Namur, Belgium.

0142-9612/02/$ - see front matter
PII: S0142-9612(02)00244-2

and Raman spectroscopy. SEM investigation was carried out with a Philips XL30 FEG scanning electron microscope equipped with an EDAX system. The accelerating voltage was 5 kV in order to ensure a limited thickness of the analysed surface layer (estimated to be about 0.25 μm for carbon and 0.1 μm for stainless steel). XRD analysis was performed using a Seifert 3003 TT diffractometer (40 kV, 30 mA, Cu K_α, grazing incidence at 1° and 10°) and Rayflex analysis software which allowed comparison of the data obtained with JCPDS powder diffraction file (PDF) database. XPS measurements were performed in commercial VG Escalab 220i-XL equipment (base pressure in the analytical chamber 10^{-8} Pa, argon pressure during sputter depth profiling 10^{-5} Pa, monochromated Al K_α X-ray source (1486.6 eV)). The high-resolution XPS spectra used for assessment of the chemical state as well as for quantification were recorded at constant pass energy of 20 eV. Data analyses and quantification were carried out by the software provided by the manufacturer. Corrections were made for the transmission function of the spectrometer. The inelastic mean free path of the electrons was assumed to scale with their kinetic energy E as $E^{0.6}$. Shirley background subtraction and Scofield sensitivity factors were implemented [9]. The XPS depth profiles were recorded by using a rastered 3 keV Ar^+ ion beam. The sputtering rate of SiO_2 under the same experimental conditions was approximately 0.01 nm/s.

Raman spectra were recorded by using a Jobin–Yvon Mole S-3000 spectrograph. The light source was an Ar laser with a wavelength 514.5 nm operated at 100 mW. The light beam was focussed to a spot of about 5 μm in size.

3. Results

3.1. Thermogravimetry

The results of the thermogravimetric measurements versus temperature show that on heating at 1°C/min heating rate, $Ni_{50}Ti_{50}$ specimens gain weight in two stages due to the oxidation as it can be seen in Fig. 1. In the 200–500°C temperature interval, the weight gain can be approximated by a linear function. Beyond 500°C such an approximation can be changed by an exponential function thus suggesting that the oxidation mechanism is different above and below 500°C.

Oxidation temperatures of 300°C and 800°C were chosen for the isothermal oxidation measurements that allow us to study the kinetics of the low- and high-temperature oxidation separately. The results of these measurements are shown in Fig. 2. It can be seen that the main oxidation at 300°C starts after 1000 s. After 80,000 s the oxidation rate has considerably slowed down and seems to have reached a saturation level. The main oxidation at 800°C starts earlier (after about 100 s) and passes through a retardation plateau around 1000 s into acceleration (Fig. 2, inset). No saturation was actually observed during 70,000 s experiment for this oxidation temperature. Parabolic oxidation can be clearly seen for 800°C of isothermal oxidation (Fig. 2).

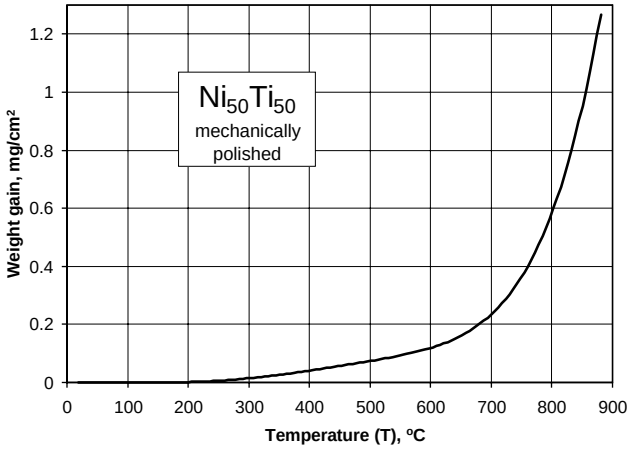

Fig. 1. Oxidation of the NiTi alloy on heating in DuPont 951 TGA with the constant rate 1°C/min and under 50 ml/min air flow. Two stages of oxidation below and above 500–600°C are distinguished.

3.2. SEM-EPMA

SEM images of specimens oxidised at 300°C, 600°C and 800°C are shown in Figs. 3 and 4, respectively. Oxidation at 300°C for half an hour resulted in the appearance of a uniform oxidised layer with regularly distributed dark spots (dimension 1–5 μm, Fig. 3a). Electron microprobe analysis was used to measure the composition of these two components on the surface. The main component, the uniform oxidised layer with the light contrast, has a composition of $Ni_{0.46}O_{0.23}Ti_{0.31}$ and the regular shaped dark spots have a composition close to TiO ($Ti_{0.55}O_{0.45}$). Chan et al. [5] also observed dark and light areas on secondary electron images of a sputter cleaned NiTi surface after 1 min of air exposure at 450°C. Using Auger point analysis, they found TiO_2 and a mixture of TiO_2 and NiO in the dark and light areas, respectively.

The surface of the samples oxidised at 400°C and 500°C was similar. However, the topography of the surface after oxidation at 600°C for half an hour was quite different (Fig. 3b). It is rougher and grainy and contains mainly Ti and O, but also a small amount of Ni. Further increase in oxidation temperature to 800°C resulted in even rougher surface (Fig. 4). The main component has a clearly visible porous structure (Fig. 4b). The composition of this component was found to have the TiO_2 stoichiometry. Against a main TiO_2 surface component, a set of flat hollows (about 100 μm

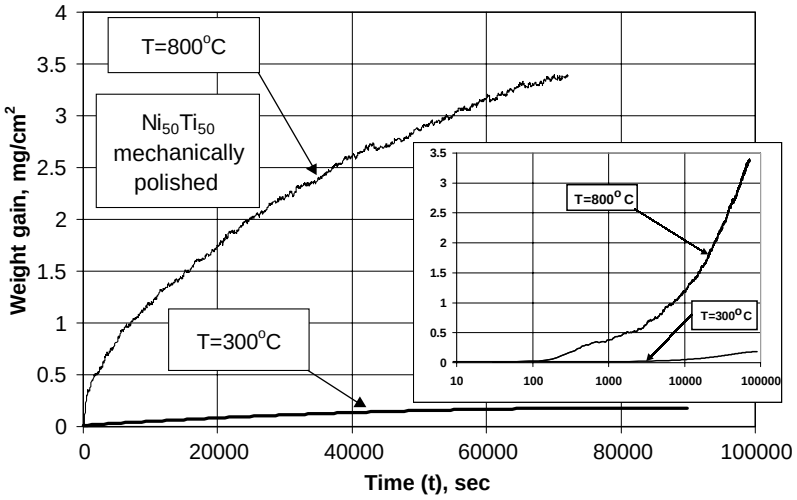

Fig. 2. Isothermal oxidation of the NiTi alloy in DuPont 951 TGA at 300°C and 800°C under 50 ml/min air flow (inset—time axis in logarithmic scale).

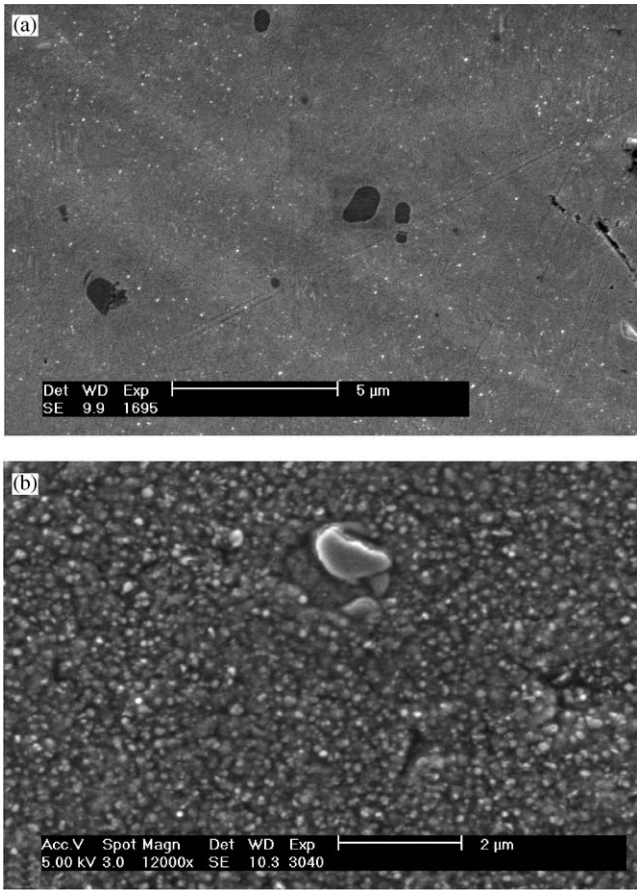

Fig. 3. SEM results for an NiTi surface oxidised for half an hour: (a) at 300°C, dark Ti oxide ($Ti_{0.55}O_{0.45}$) surrounded by the grey Ni enriched ($Ni_{0.46}O_{0.23}Ti_{0.31}$) oxidised surface; (b) at 600°C, Ti oxides (mainly TiO_2).

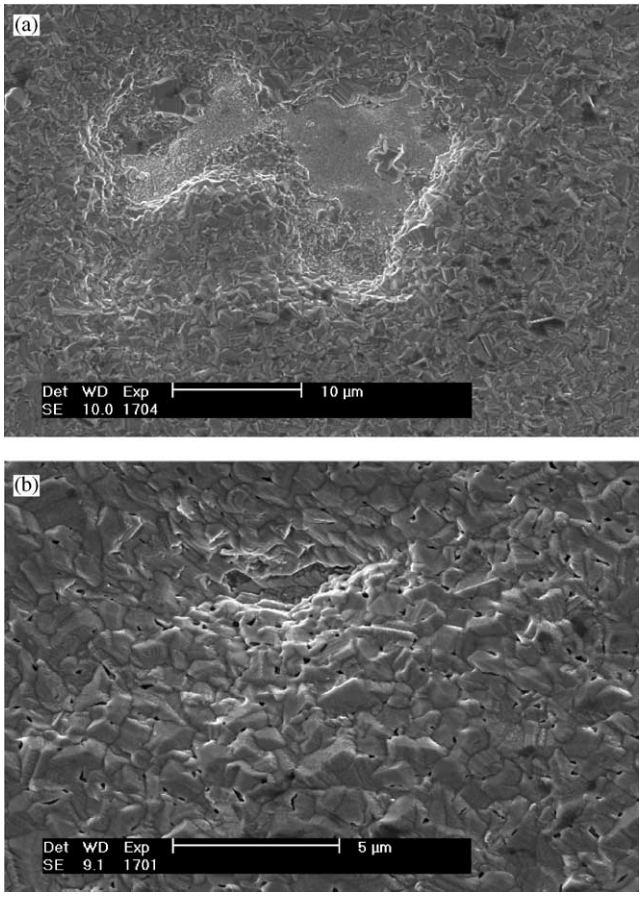

Fig. 4. SEM results for the $Ti_{50}Ni_{50}$ alloy oxidised at 800°C for half an hour: (a) Ni enriched oxidised flat hollow ($Ni_{0.4}O_{0.4}Ti_{0.2}$), (b) mainly present porous TiO_2 oxide.

between each other) can be clearly seen at low magnification (not shown). Some of the hollows have a surface morphology similar to that of the main component. However, others have a flat bottom with quite different surface morphology. An example of such a hollow is presented in Fig. 4a. Electron microprobe analysis inside the hollows revealed a chemical composition close to $Ni_{0.4}O_{0.4}Ti_{0.2}$.

3.3. Raman spectroscopy

The Raman spectra of anatase and rutile powders (Kemira Pigments), solid TiO_2 (Goodfellow) and $NiTiO_3$ powder (Aldrich Chem. Co.) were obtained as references (Fig. 5a). The anatase spectrum has peaks at 143, 197, 397, 514 and 638 cm^{-1}. The spectra of rutile powder (not shown) and that of solid TiO_2 contain peaks at 239, 447 and 612 cm^{-1}. The Raman specrtum of $NiTiO_3$ powder exhibited numerous peaks the highest of which being at 710 cm^{-1}.

Raman spectra of the surface of NiTi oxidised at 300°C, 400°C and 500°C for 30 min were quite featureless exhibiting hardly any peak. Traces of rutile were found in some spectra recorded on the NiTi surface oxidised at 600°C for 30 min. Raman spectra of the NiTi oxidised at 800°C for 30 min recorded on the flat sample surface contained the peaks of rutile (Fig. 5b, spectrum 1). Similar spectra were recorded in the hollows present in the oxide layer (Fig. 5b, spectrum 2). However, Raman spectra, recorded in some pores exhibited the peaks of rutile and $NiTiO_3$ (Fig. 5b, spectrum 3). This can be explained if we compare the Raman data with the SEM data given above. The hollows with morphology similar to the main surface obviously exhibit Raman spectra of rutile while those with smoother bottom (Fig. 4a) show the presence of $NiTiO_3$.

3.4. X-ray diffraction

The specimens oxidised at 300–800°C for half an hour were subjected to XRD analysis in order to reveal the crystal structure of the observed phases.

XRD measurements with 1° and 10° grazing incidence allowed to compare the structural composition of the upper surface layer (1°) with that of the material lying deeper (10°). After fitting the XRD pattern for an incidence angle of 1° obtained from the specimen oxidised at 300°C, it was concluded that four phases are present: TiO, hcp Ni, fcc Ni and the high-temperature NiTi B2 phase (Table 1). Structural composition did not change significantly at 10° of grazing incidence as well as with the increase of the oxidation temperature until 600°C.

A drastic change in the products of the oxidation at 600°C can be seen compared to the 300–500°C oxidation temperature interval. In the upper surface layer (Table 1, 600°C, 1° incidence angle) the strong presence of rutile (TiO_2) and Ni_3Ti intermetallic phase can be noticed instead of TiO and the B2 phase of NiTi found on the oxidised surface at lower oxidation temperatures (Table 1, 300–500°C). Some traces of the hexagonal Ni phase are still visible. Deeper X-ray penetration (Table 1, 600°C, 10° of grazing incidence) revealed the presence of the B2 and martensitic NiTi phases beneath the oxidised ($TiO_2 + Ni_3Ti + Ni$) layer.

Further increase in oxidation temperature up to 700°C results only in changes of the upper layer (Table 1, 700°C, 1° incidence angle). In addition to rutile, hexagonal Ni and bunsenite (NiO) appeared. The structural composition of the underneath layer (Table 1, 700°C, 10° incidence angle) is almost the same as the one formed at 600°C except for the absence of Ni.

Fitting of the XRD pattern taken from the NiTi alloy oxidised at 800°C revealed the presence of four main phases in the upper layer (Table 1, 800°C). The main porous structure seen during SEM measurements (Fig. 4) proved to be rutile (tetragonal TiO_2 oxide, Table 1). As for the other phases, they seem to be located beneath the rutile porous layer, only appearing on a surface in flat hollows as shown in Fig. 4.

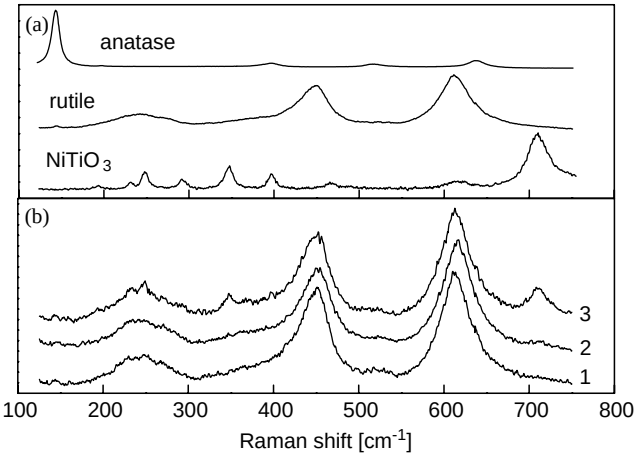

Fig. 5. (a) Reference Raman spectra: $NiTiO_3$ powder, solid TiO_2, anatase powder; (b) Raman spectra of NiTi oxidised for 30 min at 800°C, recorded on the flat surface (1) and in pores (2,3). The spectra were scaled and shifted along the *Y*-axis.

3.5. X-ray photoelectron spectroscopy

The XPS measurements showed that the freshly polished NiTi sample was covered by an oxide layer a couple of nanometers thick through which the metallic substrate was detectable. This oxide layer was composed mainly of TiO_2 but some Ti suboxides and Ni oxidised species were detected as well. The low amount of the latter did not allow us to determine their nature. The surface was relatively depleted in Ni.

The XPS depth profile of a NiTi sample oxidised at 300°C is shown in Fig. 6. It is seen that the carbon contamination on the surface was quickly removed. The oxygen concentration exhibits a peak close to the surface due to preferential sputtering of O and has a step at about 600 s of sputtering time. The titanium concentration has a maximum in the surface oxide layer, a minimum at about 600 s and reaches a steady-state value of about 39 at% due to preferential sputtering of

Table 1
Phases matched X-ray diffraction patterns taken from the NiTi alloy oxidised surface at 300–800°C

Oxidation T (°C)	PDF-no	In range	Matched	Name	Formula
300–500	2-1196	6	6	Titanium oxide (fcc)	TiO
	18-899	4	4	Nickel titanium, B2 phase	NiTi
	4-850	4	4	Nickel (fcc)	Ni
	45-1027	10	5	Nickel (hcp)	Ni
600	21-1276	21	19	Rutile, syn	TiO_2
	5-723	17	14	Nickel titanium	Ni_3Ti
	45-1027[a]	10[a]	7[a]	Nickel (hcp)[a]	Ni[a]
	18-899	4	3	Nickel titanium, B2 phase	NiTi
	35-1281	19	17	Nickel titanium, martensite	NiTi
700	21-1276	21	21	Rutile, syn	TiO_2
	5-723	17	12	Nickel titanium	Ni_3Ti
	45-1027[a]	10[a]	7[a]	Nickel (hcp)[a]	Ni[a]
	1-1239[a]	5[a]	3[a]	Bunsenite[a]	NiO[a]
	18-899	4	4	Nickel titanium, B2 phase	NiTi
	35-1281	19	16	Nickel titanium, martensite	NiTi
800	21-1276	21	21	Rutile, syn	TiO_2
	4-850	4	4	Nickel (fcc)	Ni
	33-960	30	30	Nickel titanium oxide	$NiTiO_3$
	5-723	17	14	Nickel titanium	Ni_3Ti

[a] Phases detected only at 1° of grazing incidence.
Underlined phases were additionally found at 10° of grazing incidence.
Reflections in range and matched are also shown.

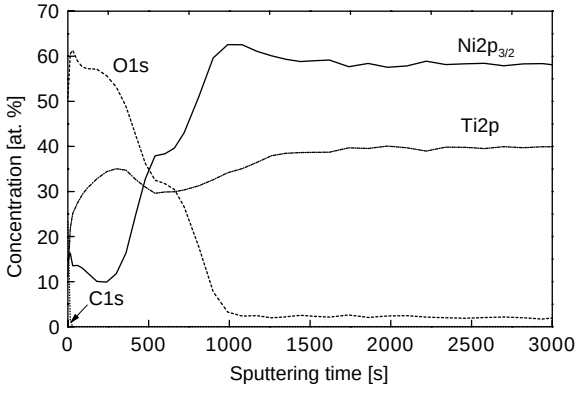

Fig. 6. XPS depth profile of an NiTi sample oxidised at 300°C for 30 min.

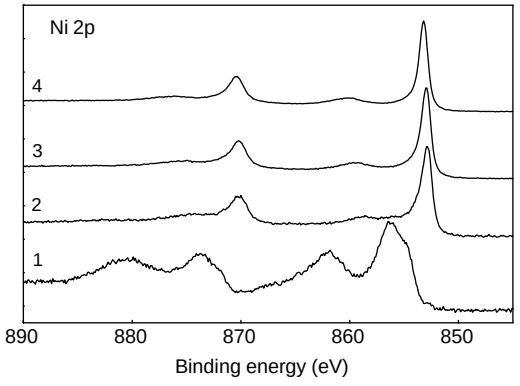

Fig. 7. Ni 2p XPS spectra of an NiTi sample treated at 300°C for 30 min: (1) as received; (2) after 60 s of sputtering; (3) after 600 s of sputtering; (4) after 1000 s of sputtering. The spectra were scaled and shifted along the Y-axis for ease of comparison.

Ti. The nickel concentration has a peak at the upper surface, passes through a minimum in the oxide layer and through a maximum just below it after about 1000 s sputtering and reaches its steady-state value of 58 at%. It is interesting to note that the Ni concentration exhibits a step in the same region (600 s) where Ti has a minimum and O has a stepwise change. This suggests the presence of a layer consisting of a ternary Ni–Ti–O phase.

The Ni 2p spectrum recorded on the surface of the 300°C treated NiTi has a peak at 856.2 eV which can be assigned either to Ni_2O_3 or to $NiTiO_3$ (Fig. 7) [9–12]. A small amount of metallic Ni was also detected. By using transmission electron diffraction Oshida et al. found that the surface oxide film formed on NiTi at 300°C in air after 10 min [13] and in pure oxygen after 30 min exposure [14] is composed mainly by TiO_2 coexisting with $NiTiO_3$. After 60 s of sputtering, the Ni 2p envelope changed drastically exhibiting the peak of metallic Ni at 852.8 eV and some remnants of oxidised Ni as a high-BE shoulder (Fig. 7). Peak fits showed that approximately 15% of the total amount of Ni was in oxidised state. From Fig. 4 in Ref. [12] we can deduce that about 40% of Ni^{2+} in $NiTiO_3$ is reduced to Ni^0 after 1 min of sputtering at similar experimental conditions. If we assume that Ni is in $NiTiO_3$ state on the NiTi oxidised surface, we can conclude that metallic Ni is present in the oxide layer. The oxidised Ni species were removed

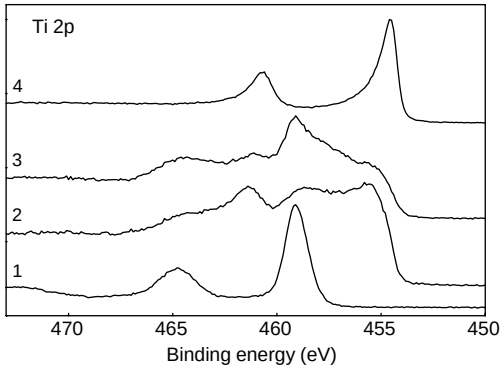

Fig. 8. Ti 2p XPS spectra of an NiTi sample treated at 300°C for 30 min: (1) as received; (2) after 360 s of sputtering; (3) reference TiO_2 after 360 s of sputtering; (4) after 1000 s of sputtering. The spectra were scaled and shifted along the *Y*-axis for ease of comparison.

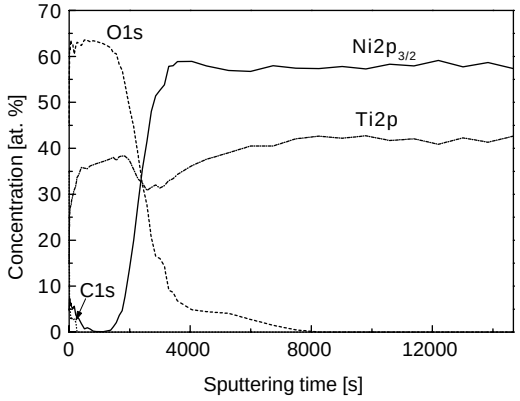

Fig. 9. XPS depth profile of an NiTi sample oxidised at 500°C for 30 min.

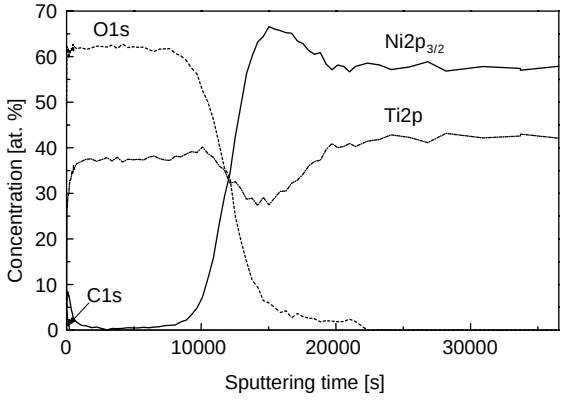

Fig. 10. XPS depth profile of an NiTi sample oxidised at 600°C for 30 min.

by further sputtering. Titanium was found as TiO_2 on the oxide surface with Ti $2p_{3/2}$ peak at 459.1 eV (Fig. 8). During depth profiling, TiO_2 is partly reduced to lower oxides. The Ti 2p spectrum of a standard TiO_2 sample (Goodfellow) sputtered under the same experimental conditions is also shown in Fig. 8 for comparison. It is seen that the Ti 2p envelope of the oxidised NiTi contains more Ti^{3+} and Ti^{2+} than the reference one indicating that Ti suboxides exist under the top layer of TiO_2.

The XPS depth profile of NiTi surface oxidised at 500°C did not exhibit steps in O and Ni dependencies (Fig. 9). The Ni concentration peaked at the surface similar to the 300°C and 400°C treated samples. However, it dropped to zero inside the oxide layer suggesting that an Ni-free layer of Ti oxides was present below the surface oxide layer enriched in Ni. A substantial tail of the O concentration was found in the alloy layer enriched in Ni lying below the oxide.

The depth profile of the NiTi sample treated at 600°C (Fig. 10) is very similar to that for the 500°C case. However, the Ni surface peak is higher and the Ni-free zone in the oxide layer is thicker. The alloy region below the oxide is more enriched in Ni and depleted in Ti than for the 500°C case.

Heat treatment of NiTi at 800°C resulted in a thick porous TiO_2 layer (cf. Fig. 4) with low content of Ni (<1 at%) in oxidised state (depth profile not shown). After a short sputtering time the XPS peak of metallic Ni was detected. Ni concentration increased to about 1% and remained almost constant during profiling. The oxide–alloy interface could not be reached even after 80,000 s sputtering time.

Ti 2p and Ni 2p spectra recorded during depth profiles of the samples treated at 400–800°C behaved in a way similar to that for the 300°C case. Titanium was found on the surface as TiO_2 that was reduced to lower oxides by sputtering. Comparison with the reference Ti 2p spectra of TiO_2 revealed that the reduction of the thermally grown oxides was faster indicating that defective TiO_2 or Ti suboxides were formed inside the films. Ni $2p_{3/2}$ peaks at the surface were at 856.2 eV characteristic of Ni_2O_3 or $NiTiO_3$. During depth profiling the peak of metallic Ni emerged while that of oxidised Ni strongly decreased. This process was faster for the 400°C treated surface indicating the possible presence of some metallic Ni in the oxide layer. More oxidised Ni species were found in the oxide films for temperatures of 500°C and higher. However, the presence of metallic Ni in the oxide layers for those cases cannot be excluded.

The data on the surface composition of NiTi samples oxidised at different temperatures for 30 min is summarised in Table 2. Carbon contamination was present on all samples. The freshly polished NiTi surface had the highest Ni content while that treated at 800°C had the lowest one.

The thickness of the oxide layers formed on NiTi during 30 min of oxidation at different temperatures as determined from the XPS depth profiles is shown in Fig. 11 as an Arrhenius plot. It is seen that a significant

change in the oxidation rate takes place in the temperature range above 400°C. The data presented show a similar trend as the weight gain versus temperature (cf. Fig. 1).

Table 2
Surface composition (at%) of NiTi samples oxidised at different temperatures

	Ni $2p_{3/2}$	Ti 2p	O 1s	C 1s
As polished	20	15	28	37
300°C	15	51	11	23
400°C	7	18	53	22
500°C	4.5	15	45.5	35
600°C	5	15	50	30
800°C	0.3	11	34.7	54

XPS lines used for quantification are indicated.

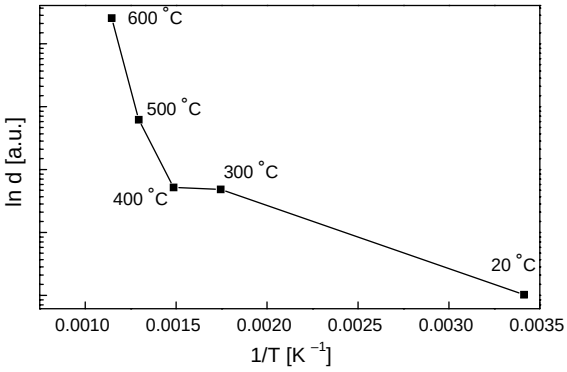

Fig. 11. Thickness of oxide layers (30 min oxidation time) on NiTi versus oxidation temperature as determined by XPS depth profiles. Solid lines are drawn to guide the eye.

3.6. Thermodynamic calculations

The vertical section NiTi–O (Fig. 12) of the Ni–Ti–O system was calculated using the ThermoCalc [15] databank system. The required Gibbs energy data are taken from the literature [16–19]. The calculations are made under the assumption that oxygen is insoluble in the compounds NiTi and Ni_3Ti and that nickel is similarly insoluble in the oxides of titanium. The calculations indicate that towards the surface (NiTi/air interface) one would expect $NiTiO_3$, TiO_2, and metallic Ni. NiO may not be formed, as this would require higher oxygen pressures. Below the surface layer one would expect lower oxides of Ti and Ni_3Ti.

4. Discussion

The XPS data for the NiTi surface oxidised at 300°C suggest that a mixture of TiO_2 and $NiTiO_3$ was present on the gas–oxide interface. A layer containing Ti suboxides (TiO) and metallic Ni (both hcp and fcc) and possibly partly oxidised Ni is situated below that surface layer, the Ni concentration having a minimum (Fig. 6). According to the results of XRD analysis, Ni enriched B2 phase region of the NiTi alloy at the oxide/metal interface follows (Table 1).

It can be suggested that titanium being the more reactive element, segregates to the surface and is oxidised there forming TiO_2 [20] with an Ni enriched alloy layer underneath. The Ti oxide layer formed contains Ti suboxides below the TiO_2 on the gas/oxide

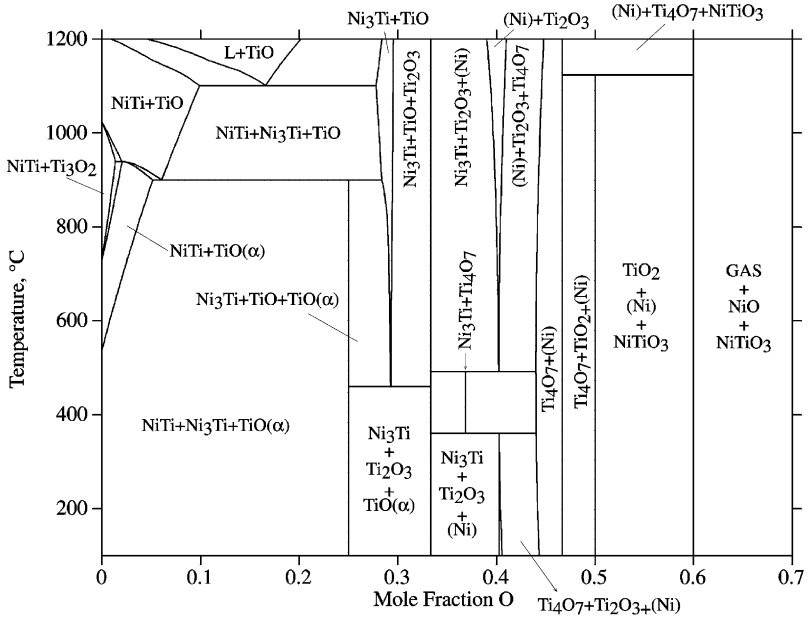

Fig. 12. Calculated equilibrium phase diagram of NiTi–O.

interface similar to the oxidation of pure Ti [21]. Then diffusion of Ni to the surface takes place followed by its partial oxidation. There may be several reasons for this: stresses induced due to Ti oxide formation, surface energy decrease or oxidation of Ni. It was shown that Ni atoms in metallic state diffuse easily through defective TiO_x [22]. On the other hand, the Ti oxide layer formed in the case of NiTi oxidation at 300°C is protective because the oxidation rate seems to slow down significantly with time (Fig. 2, 300°C). Moreover, according to the XRD data analysis, in the 300–500°C temperature range of oxidation, a mixture of TiO, Ni (fcc), Ni (hcp) and B2 NiTi phases is present on the surface (Table 1). TiO_2 and $NiTiO_3$ are in this case not detectable by XRD because the sensitivity of the technique is not sufficient. The presence of these phases is generally in agreement with the calculated NiTi–O equilibrium phase diagram (cf. Fig. 12). It is visible that for the low temperature of oxidation (below 500°C) not more than 0.1 of the oxygen mole fraction can be present in a layers just above the B2 NiTi phase according to the phase diagram (cf. Fig. 12) and the observed phase composition (Table 1).

The phase transition from the fcc to hexagonal nickel may take place because of the internal compressive stresses that work like hydrostatic pressure which can promote the formation of the hexagonal phase analogously to cobalt fcc↔hcp transformation. It was established that large compressive stresses exist in the NiO formed on Ni [23]. Ni that appeared already on a surface has transformed back to the normal fcc phase. Such a transition can decrease the driving force for the Ni and oxygen diffusion and result in the "saturation" of the oxidation observed at 300°C (Fig. 2).

The oxidation rate of NiTi changes considerably at temperatures higher than 400–500°C (cf. Fig. 1 and Fig. 11). The depth profiles also change their shape. After oxidation at 500°C the minimum in Ni content in the oxide layer reaches zero (Fig. 9), which means that only the Ni at the air/rutile interface will be eventually released after the implantation of the NiTi oxidised in such a manner. A possible explanation of the different oxidation behaviour of NiTi below and above 500°C could be the decomposition of Ti oxide by the neighbouring metallic Ti at the oxide/alloy interface. According to Bui et al. [24], such decomposition takes place during oxidation of Ti at temperatures above 350°C. It creates a high density of vacancies allowing fast diffusion of oxygen resulting in linear or quasi-linear oxidation of Ti. In the case described in this article a similar process could lead to an increase of the oxidation rate.

At 600°C the nickel content minimum in the oxide layer is much broader but titanium oxide thickness without Ni is smaller than at 500°C. Oxygen delivery to the underneath layers is much deeper compared to 500°C oxidation (Figs. 9 and 10). Ni_3Ti and NiTi martensite were detected by XRD instead of fcc Ni. The most important difference, however, is the formation of the stable rutile instead of the metastable TiO oxide not only in a few nanometers at the air/oxide interface but also in depth (Table 1). It seems that the temperature of 600°C is high enough to allow vacancies to assemble and form cavities and pores in the rutile layer as it was suggested in [25]. The SEM studies also confirmed the change of the surface morphology from smooth at 300–500°C (Fig. 3a) to rough and finally porous at 600–800°C (Figs. 3b and 4). Comparisons of the calculated NiTi–O equilibrium phase diagram (cf. Fig. 12) with phase composition in these two temperature regions of oxidation (Table 1) also give us an indirect evidence of the drastic change in oxygen delivery to the layers above NiTi. One can see (Table 1) that we did not detect Ti suboxides like Ti_2O_3 or Ti_4O_7 predicted by the equilibrium calculations (cf. Fig. 12). It means that in the 500–600°C temperature range, the amount of oxygen in the layers above NiTi jumps from approximately 0.1 to more than 0.5 mole fraction of oxygen. Another confirmation of the change in the oxidation mechanism at 500–600°C temperature range can be found in Fig. 1 where the weight gain accelerates at temperatures higher than 500°C. This is also evident from Fig. 11 representing the thickness of oxide layers which is growing rapidly at temperatures above 400°C. One should not mix it up with the isothermal parabolic oxidation that took place indeed (Fig. 2) which is in good agreement with [25]. All these facts testify to the ease of oxygen delivery to the underneath layers above 500°C of oxidation.

Oxidation at 800°C resulted in formation of porous TiO_2 rutile on the air/oxide interface ensuring the increase in the oxygen delivery to the underneath layers. At 800°C rutile is found together with $NiTiO_3$, which is in good agreement with the thermodynamic calculations and is also confirmed by the Raman (Fig. 5), SEM (Fig. 4) and XRD measurements (Table 1). It seems also that as the rutile becomes thicker it starts to crack exposing an underneath layer with a different surface morphology containing rutile and $NiTiO_3$. As far as the Ni enriched alloy layer under the oxide film is concerned, this is the result of segregation of Ti during the oxidation as can be seen from XRD analysis (Table 1).

The austenitic cubic unoxidised NiTi B2 phase can be detected beneath the oxides for the temperature range 300–500°C (Table 1). It indicates that NiTi bulk material was depleted by Ti. This was confirmed by the XPS depth profiles (cf. Figs. 6 and 9). As a result, the martensitic transformation temperature dropped below room temperature, otherwise we should have detected not the austenite but the monoclinic B19′ martensitic phase. At 800°C such depletion in Ti was so strong that

instead of austenitic NiTi we observed even the Ni_3Ti intermetallic phase (Table 1).

5. Conclusions

- NiTi alloy exhibits different oxidation behaviour in air at temperatures below and above 500°C. In the lower temperature range a layer of TiO and metallic fcc and hcp nickel is formed covered by a TiO_2 layer with $NiTiO_3$. The oxide scale is smooth and protective and the oxidation rate is relatively low. At temperatures of 600°C and above, rutile is formed at the air/oxide interface with a layer containing $NiTiO_3$ below when oxidised at 800°C. The surface becomes rough (600°C) and the top rutile layer has a clearly visible porous structure (800°C).
- Ni concentration has a peak at the air/oxide interface and a minimum in the oxide layer for samples oxidised at 300–600°C. The amount of Ni detected on the surface decreases with the rise of the oxidation temperature. An Ni-free zone was found in the oxide layer for oxidation temperatures of 500°C and 600°C.
- The martensitic transformation of the substrate NiTi alloy beneath the oxidised scale is suppressed below room temperature because of the depletion of the NiTi lattice by Ti which is consumed in the oxidised scale to produce Ti oxides. An Ni_3Ti phase starts to precipitate in the Ti-depleted NiTi layer when treated above 600°C.
- The oxidation treatment of NiTi in air at temperatures close to 500°C produces a smooth protective nickel-free oxide layer which is in favour of good biocompatibility of NiTi implants.

Acknowledgements

R.G.V. and B.B. kindly acknowledge the financial support of the Foundation for Scientific Research, Flanders.

References

[1] Duerig T, Pelton A, Stöckel D. An overview of nitinol medical applications. Mater Sci Eng 1999;A273–275:149.
[2] Van Humbeeck J, Stalmans R, Besselink PA. In: Helsen JA, Breme HJ, editors. Metals as biomaterials. Chichester: Wiley, 1998. p. 73–100.
[3] Shabalovskaya SA, Anderegg JW. Surface spectroscopic characterization of TiNi equiatomic shape memory alloys for implants. J Vac Sci Technol 1995;A13:2624–32.
[4] Shabalovskaya SA. Biological aspects of TiNi alloy surfaces. J Phys IV 1995;5:C8-1199–204.
[5] Chan CM, Trigwell S, Duerig T. Oxidation of a NiTi alloy. Surf Interface Anal 1990;15:349–54.
[6] Trigwell S, Hayden RD, Nelson KF, Selvaduray G. Effects of surface treatment on the surface chemistry of NiTi alloy for biomedical applications. Surf Interface Anal 1998;26:483–9.
[7] Thierry B, Tabrizian M, Savadogo O, Yahia L'H. Effects of sterilization processes on NiTi alloy: surface characterization. J Biomed Mater Res 2000;49:88–98.
[8] Vichev RG, Yong Liu, Van Humbeeck J, Blanpain B, Celis JP. Thermally grown oxide films on NiTi shape memory alloys. In: Olefjord I, Nyborg L, Briggs D, editors. Proceedings of the Seventh European Conference on Applications of Surface and Interface Analysis ECASIA'97, Goteborg, June 1997. Chichester: Wiley, 1997. p. 679–82.
[9] Briggs D, Seah MP, editors. Practical surface analysis, vol. 1: Auger and X-ray photoelectron spectroscopy. Chichester: Wiley, 1990.
[10] Malherbe JB, Hoffmann S, Sanz JM. Preferential sputtering of oxides: a comparison of model predictions with experimental data. Appl Surf Sci 1986;27:355–65.
[11] Gonzales-Elipe AR, Munuera G, Espinos JP, Sanz JM. Compositional changes induced by 3.5 keV Ar+ ion bombardment in Ni–Ti oxide systems: a comparative study. Surf Sci 1989;220:368–80.
[12] Leinen D, Fernandez A, Espinos JP, Gonzales-Elipe AR. XPS and ISS study of $NiTiO_3$ and $PbTiO_3$ subjected to low-energy ion bombardment. Surf Interface Anal 1993;20:941–8.
[13] Oshida Y, Miyazaki S. Corrosion and biocompatibility of shape memory alloys. Corros Eng 1991;40:1009–25.
[14] Oshida Y, Sachdeva R, Miyazaki S. Changes in contact angles as a function of time on some pre-oxidised biomaterials. J Mater Sci: Mater Med 1992;3:306–12.
[15] Sundman B, Jansson B, Andersson J. The Thermo-Calc databank system. Calphad 1985;9:153–90.
[16] Dinsdale AT. SGTE data for pure elements. Calphad 1991;15:317–425.
[17] Lee B-J, Saunders N. Thermodynamic evaluation of the Ti–Al–O ternary system. Z Metallkd 1997;88:152–61.
[18] Kowalski M, Spencer PJ. Thermodynamic reevaluation of the Cr–O, Fe–O and Ni–O systems—remodeling of the liquid, bcc and fcc phases. Calphad 1995;19:229–43.
[19] The Scientific Group Thermodata Europe (SGTE), substance database, 1998.
[20] McBreen PH, Polak M. An Auger study of the adsorption of oxygen on TiNi, TiFe and Ti_4Fe_2O. Surf Sci 1987;179:483–97.
[21] Rogers Jr JW, Erickson KL, Belton DN, Springer RW, Taylor TN, Beery JG. Low temperature diffusion of oxygen in titanium and titanium oxide films. Appl Surf Sci 1988–89;35:137–52.
[22] Espinos JP, Fernandez A, Gonzales-Elipe AR. Oxidation and diffusion processes in nickel–titanium oxide systems. Surf Sci 1993;295:402–10.
[23] Stout JH, Shores DA, Goedjen JG, Armacanqui ME. Stresses and cracking of oxide scales. Mater Sci Eng 1989;A120:193–7.
[24] Bui Minh Duc, Jardin C, Gauthier JP, Thollet G, Michel P. Oxidation mechanism, oxide decomposition and phase transition in industrial titanium studied by high resolution low energy electron spectrometry. In: Kimura H, Izumi O, editors. Titanium'80: Proceedings of the Fourth International Conference on Titanium, Kyoto, vol. 4, May 1980, Warrendale, USA: The Metallurgical Society of AIME, 1980. p. 2821–7.
[25] Chu CL, Wu SK, Yen YC. Oxidation behavior of equiatomic TiNi alloy in high temperature air environment. Mater Sci Eng 1996;A216:193–200.